Hindawi
Mathematical Problems in Engineering
Volume 2018, Article ID 2381370, 10 pages
https://doi.org/10.1155/2018/2381370

Research Article

Stability Analysis of Three-Dimensional Slopes Considering the Earthquake Force Direction

Yukuai Wan, Yufeng Gao, and Fei Zhang

Key Laboratory of Ministry of Education for Geomechanics and Embankment Engineering, Hohai University, No. 1, Xikang Road, Nanjing, 210098, China

Correspondence should be addressed to Yukuai Wan; wanyukuai@163.com

Received 7 August 2018; Revised 30 October 2018; Accepted 10 November 2018; Published 2 December 2018

Academic Editor: Francisco J. Montáns

Simplified 3D Spencer's method is proposed to evaluate the stability of slopes under earthquake force and a random search algorithm is used to determine the critical slip surface. A computer code was written in Matlab to determine the critical slip surface and calculate its safety factor and direction of sliding (DOS). The applicability of the presented code is verified by reanalyzing three slope stability problems. Then, a comparison is made to investigate the effects of the direction of earthquake force on the factor of safety and the DOS of the critical slip surface. Accounting for the effects of the direction of earthquake force, the difference in safety factors, and the DOS can be up to 40% and 40°, respectively. Finally, a parametric study is also conducted to determine the effects of the soil strength parameters (c', φ'). It is found that the effective cohesion c' and friction angle φ' of the soil have nearly no influence on the unique DOS of the critical surface. Application of the presented approach into 3D slopes under quasistatic load is straightforward.

1. Introduction

Estimating the slope stability remains one of the most important problems for geotechnical engineers. Slope stability analyses have usually been performed using two-dimensional (2D) simulation [1–4]. However, in most cases, the geometry of the slopes has three-dimensional (3D) characteristics, such as corners, conical heaps, and dams in narrow valley. Traditional 2D methods do not consider 3D effects resulting conservatism in the analysis of slope stability under complex condition [5].

Recently, various 3D slope stability methods have been proposed to obtain more reasonable solutions. These 3D analysis methods can be divided into three categories: limit equilibrium method, limit analysis method, and finite element method. The limit equilibrium method is most widely used in practice to analyze the stability of slopes. A number of 3D limit equilibrium methods, based on simple extension of convention 2D methods, have been proposed to estimate the 3D effects on the safety of slope [6–8]. All these methods assumed the sliding body to move along the plane of symmetry. Such an assumption, however, can lead to miscalculation of the factor of safety for slopes under asymmetrical conditionals, such as the complex geometry, variable soil stratigraphy, external loading, seismic forces, or other factors [9, 10].

Huang and Tsai [9] introduced the DOS that defines the direction of movement of the sliding mass in the horizontal plane and proposed a new 3D Bishop's method that satisfies two-direction moment equilibrium. Based on this new concept of 'two-direction equilibrium', a number of researchers proposed various 3D asymmetrical slope stabilities analysis methods [10, 13–15]. Among these methods, simplified Spencer's method proposed by Wan et al. [15] satisfies all the force equilibrium and two-direction moment equilibrium. This method has relatively rigorous theoretical basis. The method presented by Wan et al. [15] is further exploited to investigate the stability of 3D slopes under quasistatic load.

Slope failure induced by earthquake loads can lead to serious damage and loss of lives. For example, the Wenchuan earthquake (Ms=8.0) on May 12th, 2008, directly caused more than 15000 landslides which resulted in more than 20000 deaths. Since the mid-1970s, increasing attention has been directed toward the stability analysis of slopes under

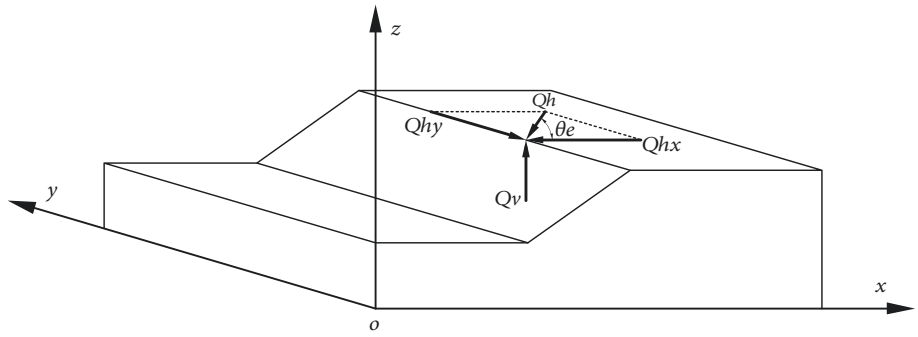

Figure 1: Direction of earthquake force.

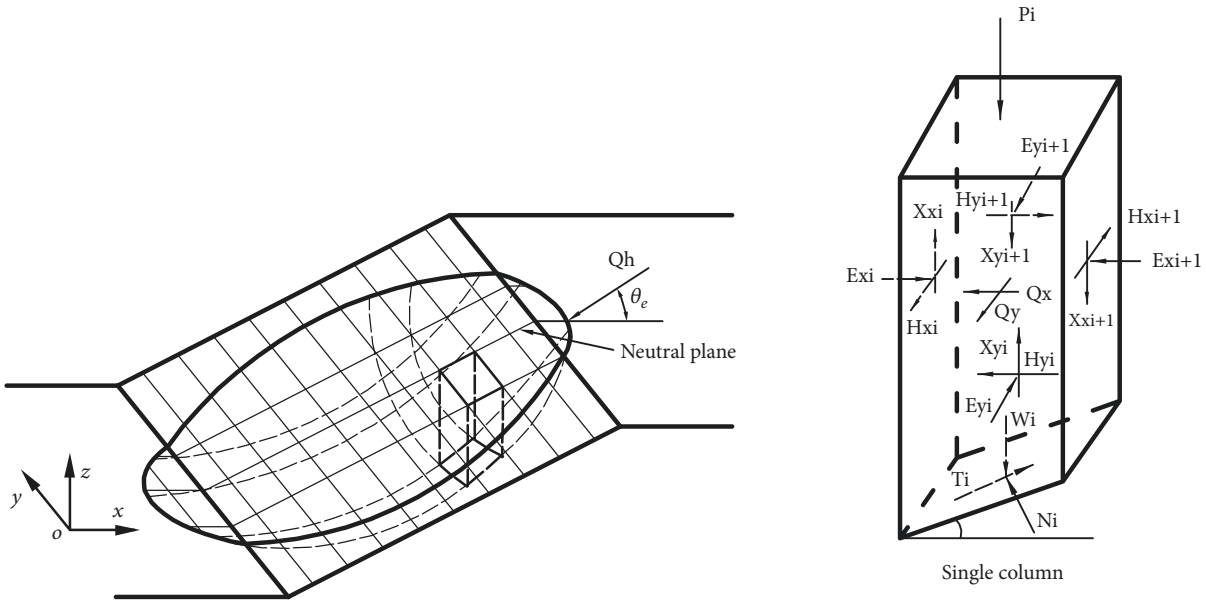

Figure 2: Discretization of a failure mass.

earthquake forces [17–19]. At present, there are four methods for seismic stability analysis of slopes: pseudo-static method, Newmark sliding block analysis method, numerical analysis method, and testing method. The conventional pseudo-static method is still widely applied for evaluating the effects of earthquake forces on the stability of a slope [20, 21]. Under three-dimensional conditions, earthquake forces can act in all three directions-along two horizontal directions (x and y) and the vertical direction (z) as shown in Figure 1. Most of the pseudostatic analyses have involved the consideration of the horizontal earthquake force $Q_{h,}$ and vertical earthquake force Q_v. However, previous studies assumed that the horizontal earthquake force Q_h is parallel to the x-axis and neglected the effects of the direction of earthquake force θ_e on the slope safety. To improve the accuracy of 3D slope stability analysis, the effects of the direction of the earthquake force on 3D slope stability analysis should be taken into account.

In this paper, the method presented by Wan et al. [15] is further exploited to evaluate the stability of 3D slopes under quasistatic load. An efficient optimization method proposed by Chen [22] is attempted to determine the critical slip surface of slopes. The effect of the direction of the earthquake force on the factor of safety and the DOS of the critical slip surface is also investigated. The difference in factor of safety and the DOS is compared to investigate the effects of the direction of earthquake force on the safety of 3D slopes. A parametric study is also conducted to show the effects of the soil strength parameters (effective cohesion c', effective friction angle φ') on the DOS of the critical slip surface.

2. Formulation of 3D Spencer's Method

As with other 3D limit equilibrium methods, the potential failure mass of a slope is discretized into a number of columns with vertical interface. Figure 2 illustrates the internal and external forces acting on the various faces of the column ith. To establish the force and moment equilibrium equations, the following assumptions are included:

(1) The conventional definition for factor of safety F reduces the available shear strength parameters c' and

ϕ' by the following equations to bring the slope to a limiting state.

$$c'_d = \frac{c'}{F} \tag{1}$$

$$\tan \phi'_d = \frac{\tan \phi'}{F} \tag{2}$$

where c' and ϕ' are the effective cohesion and friction angle of the soil, respectively; c'_d and ϕ'_d are soil strength parameters necessary to maintain the structure in limit equilibrium, respectively.

(2) The horizontal shear forces, H_{xi} and H_{zi}, are assumed to 0. Such an assumption was also adopted by Hungr [6], Huang and Tsai [9] and Cheng and Yip [10]. The following relationships between the intercolumn vertical shear forces (X_{xi} and X_{yi}) and the normal force (E_{xi} and E_{yi}) of ith column are assumed:

$$X_{xi} = E_{xi}\lambda_x \tag{3}$$

$$X_{yi} = E_{yi}\lambda_y \tag{4}$$

where λ_x and λ_y are shear force factors in the x- and y-directions, respectively.

(3) Soil columns are assumed to move in the same direction, i.e. the DOS is unique on the x-y plane for all columns. The unique DOS, a, is equal to the angle between positive x-axis and the projection of the shear force T_i on the base of each soil column in x-y plane (measured counterclockwise from the positive x-axis).

(4) The pseudostatic method is adopted by the writers in the present formulation and by many other researchers [20, 21]. The horizontal earthquake force, Q_{hi}, is assumed to act towards the center of the column. The components of the horizontal earthquake forces, Q_{hxi} and Q_{hyi}, can be expressed as

$$Q_{hxi} = Q_{hi} * \cos(\theta_e) = W_i * K_h * \cos(\theta_e) \tag{5}$$

$$Q_{hyi} = Q_{hi} * \sin(\theta_e) = W_i * K_h * \sin(\theta_e) \tag{6}$$

where K_h is the pseudostatic acceleration coefficient and θ_e is the angle between positive x-axis and the earthquake force Q_{hi} (measured counterclockwise from the positive x-axis).

The unit vector, (m_{xi}, m_{yi}, and m_{zi}), for the shear force T_i of the ith column can be determined by

$$\begin{gathered} m_x^2 + m_y^2 + m_z^2 = 1 \\ m_x * n_x + m_y * n_y + m_z * n_z = 0 \\ m_x = \tan a * m_y \end{gathered} \tag{7}$$

where (n_{xi}, n_{yi}, n_{zi}) is unit vector for the normal force N_i of the ith column.

Establish the vertical and horizontal force equilibrium for the ith column in x, y, and z-directions, as

$$\begin{aligned} &-W_i + N_i * n_{zi} + T_i * m_{zi} + X_{xi} - X_{xi+1} + X_{yi} \\ &\quad - X_{yi+1} = 0 \end{aligned} \tag{8}$$

$$N_i * n_{xi} + T_i * m_{xi} + E_{xi} - E_{xi+1} - Q_{hxi} = 0 \tag{9}$$

$$N_i * n_{yi} + T_i * m_{yi} + E_{yi} - E_{yi+1} - Q_{hyi} = 0 \tag{10}$$

By substituting (3), (4), (9), (10), and Mohr-Coulomb's failure criterion 12 into (8), the effective normal force, $N_{i,}$, can be expressed as

$$N_i = \frac{W_i - Q_{hxi} * \lambda_x - Q_{hyi} * \lambda_y + \left(u_i * A_i * \tan \phi'_d - c'_d * A_i\right) * \left(-m_{xi} * \lambda_x - m_{yi} * \lambda_y + m_{zi}\right)}{-n_{xi} * \lambda_x - n_{yi} * \lambda_y + n_{zi} + \tan \phi'_d * \left(-m_{xi} * \lambda_x - m_{yi} * \lambda_y + m_{zi}\right)} \tag{11}$$

where A_i is the area of the column base.

The shear force T_i can be determined by application of Mohr-Coulomb's failure criterion.

$$T_i = \left(N_i - u_i * A_i\right) * \tan \phi'_d + c'_d * A_i \tag{12}$$

Considering the overall force equilibrium in the x- and y-directions

$$S = \sum \left(N_i * n_{xi} + T_i * m_{xi} - Q_{hxi}\right) = 0 \tag{13}$$

$$Z = \sum \left(N_i * n_{yi} + T_i * m_{yi} - Q_{hyi}\right) = 0 \tag{14}$$

Establishing the overall moment equilibrium equation about the x- and y-axis, respectively,

$$\begin{aligned} M_y = \sum \big(&-W_i * x_i + Q_{hxi} * z_{ei} - N_i * n_{xi} * z_i + N_i \\ &* n_{zi} * x_i - T_i * m_{xi} * z_i + T_i * m_{zi} * x_i\big) = 0 \end{aligned} \tag{15}$$

$$\begin{aligned} M_x = \sum \big(&-W_i * y_i + Q_{yi} * z_{ei} - N_i * n_{hyi} * z_i + N_i \\ &* n_{zi} * y_i - T_i * m_{yi} * z_i + T_i * m_{zi} * y_i\big) = 0 \end{aligned} \tag{16}$$

where x_i, y_i, and z_i are coordinate values of the center of a column base; z_{ei} is the z- coordinate of the center of a column. The unknowns, namely, F, λ_x, λ_z, and a, can be obtained by

solving the system of equations consisting of (13), (14), (15), and (16).

The presented Spencer's method can be simplified to Bishop's method by considering only moment equilibrium equations (15) and (16) about axes parallel to x- and y-axis direction, respectively. Similarly, presented Spencer's method can be simplified to Janbu's simplified method by considering only force equilibrium equations (13) and (14) in x- and y-axis direction, respectively. One more assumption that the intercolumn vertical shear force (X_{xi} and X_{yi}) is neglected is made in Bishop's and Janbu's simplified method. The normal force N_i can be expressed as

$$N_i = \frac{W_i + \left(u_i \bullet A_i \bullet \tan\phi'_d - c'_d \bullet A_i\right) \bullet m_{zi}}{n_{zi} + \tan\phi'_d \bullet m_{zi}} \tag{17}$$

3. Optimization Procedure

The studies dealing with slope stability analysis within the framework of limit equilibrium involves two sequential steps: calculating the factor of safety for a given slip surface and determining the critical slip surface and its corresponding minimum factor of safety. Factor of safety is calculated by the proposed limit equilibrium method. Optimization process is used to determining the shape and location of the critical slip surface. The slip surface is commonly assumed to be a particular shape, such as spherical, ellipsoidal, and nonuniform rational B-splines. This paper introduces a general ellipsoidal shape as the shape of failure in 3D analysis. This ellipsoid can rotate on the x-y plane and the rotated ellipsoid is presented as equation.

$$\begin{aligned}&\frac{\left[\cos\theta * (x - X_c) - \sin\theta * (y - Y_c)\right]^2}{R_x^2} \\ &\quad + \frac{\left[\cos\theta * (y - Y_c) + \sin\theta * (x - X_c)\right]^2}{R_y^2} \\ &\quad + \frac{(z - Z_c)^2}{R_z^2} = 1\end{aligned} \tag{18}$$

where θ is the rotation angle of the ellipsoid in the x–y plane; X_c, Y_c, and Z_c, are coordinates of the center of the ellipsoid in the x-, y-, and z-directions, respectively; R_x, R_y, and R_z are semiradiuses of the ellipsoid in the x-, y-, and z -directions, respectively.

An optimization technique proposed by Chen [22] that was found to be effective in previous work by Gao et al. [23] is used to find the minimum factor of safety. In this technique, a random search algorithm is used to find an initial estimate slip surface as the starting point in search of the global minimum, and then a minimization procedure is carried out until the bandwidths of the search variables become less than predefined values. The procedure is proposed to consist of the following steps.

Step 1. Generate a slip surface $Z^0(Xc, Yc, Zc, Rx, Ry, Rz, \theta)$ and calculate its factor of safety F_0.

Step 2. Generate a new slip surface Z^1 and its factor of safety F_1. The coordinates of Z^1 are determined by

$$Z_i^1 = Z_i^0 + l_i \bullet u\,(0, 1) \tag{19}$$

where Z^1 is a new slip surface; l_i is the bandwidths of the search variables; $u(0,1)$ is a random number ranging between -1 and 1.

Step 3. Compare F_0 and F_1. If $F_1 \leq F_0$, Z^0 and F_0 are replaced by Z^1, F_1, respectively.

Step 4. Repeat Steps 2-3 and Z^0 and F_0 are renewed until the number of trials reached a specified value N, then $l_i = l_i/2$.

Step 5. Repeate Step 4 until the $l_i < \varepsilon$.

4. Results and Discussion

Example 1. Example 1 is a homogeneous, laterally symmetrical slope. The geometry and material properties of Example 1 are shown in Figure 3. This example was analyzed by Zhang [16] using Bishop's, Janbu's simplified and Spencer's method. In these methods, a special ellipsoid slip surface (R_y=R_x, θ=0) was employed to determine the critical slip surface and its corresponding minimum factor of safety. The same example was performed to verify the performance of random search method in determining the minimum factor of safety.

Based on Bishop's, Janbu's simplified, and Spencer's method, random search method was applied to determine the critical slip surface and the corresponding minimum factor of safety. The results obtained by the presented method, compared to those provided by Zhang [16] using Bishop's, Janbu's simplified, and Spencer's method are listed in Tables 1, 2, and 3, respectively. The calculated DOS are equal to 0°, which is the same as expect. The critical slip surface obtained by the presented method and those provided by Zhang [16] are illustrated in Figure 4. It can be seen from Tables 1, 2, and 3 that the minimum factors of safety obtained by presented method is slightly smaller than those provided by Zhang [16].

Example 2. Example 2 is performed to validate the performance of the random research in determining the minimum factor of safety and its corresponding critical slip surface. This example was first analyzed by Alkasawneh et al. [11] to study the effects of different search techniques on the minimum factor of safety and was reanalyzed by Kalatehjari et al. [12] to verify the application of particle swarm optimization (PSO). Figure 5 illustrates the geometry, strength parameters, and unit weight of Example 2. For validation, a comparison of the minimum safety factors is summarized in Table 4. The critical slip surface obtained by presented method is illustrated in Figure 6. The results obtained by the presented study are close to those of Alkasawneh et al. [11] and Kalatehjari et al. [12]. The difference between the result of this study and that of Kalatehjari et al. [12] is 1.6%. Moreover, the difference between the results of current study and the results proposed by Alkasawneh et al. [11] for 2D and 3D analysis are 0.18% and

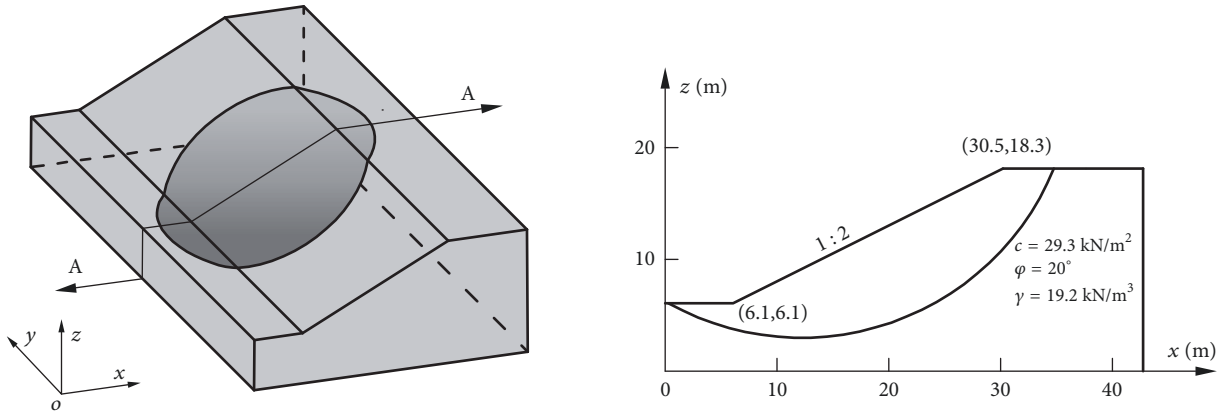

Figure 3: Geometry and properties of Example 1.

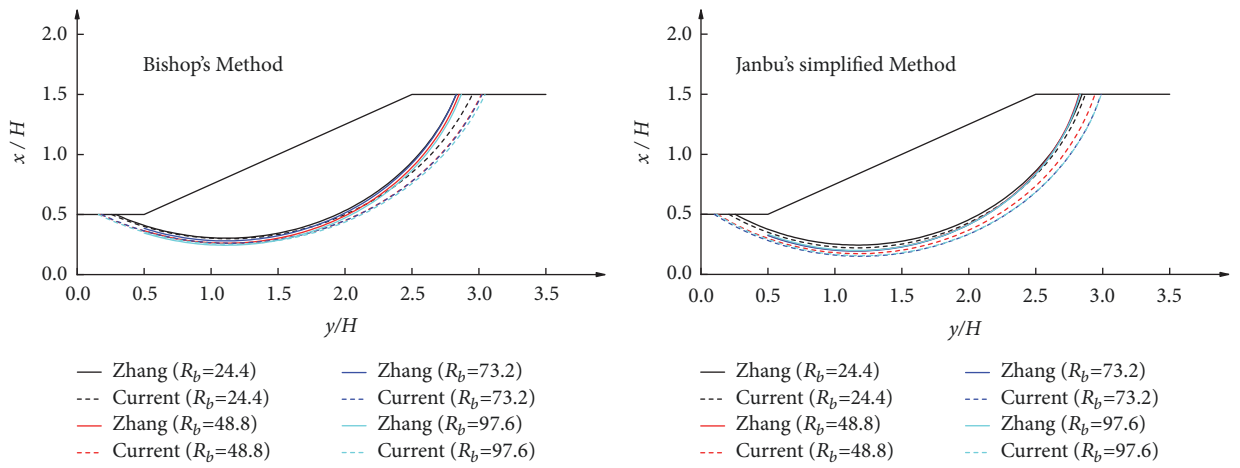

(a) Comparison of the critical slip surface for Bishop's method

(b) Comparison of the critical slip surface for Janbu's simplified method

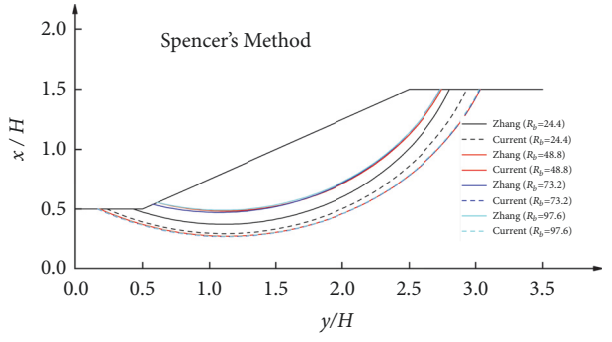

(c) Comparison of the critical slip surface for Spencer's method

Figure 4: The calculated critical slip surface compared with those provided by Zhang [16].

Table 1: Comparisons of F and critical slip surface for Example 1 (Bishop's method).

R_y (m)	24.4		48.8		73.2		97.6	
	Zhang	Current	Zhang	Current	Zhang	Current	Zhang	Current
F	2.246	2.237	2.155	2.133	2.133	2.112	2.130	2.104
X_c (m)	13.59	13.76	13.57	13.88	13.52	13.94	13.52	13.93
Z_c (m)	26.01	27.83	25.64	28.12	25.67	28.14	25.68	28.42
R_x (m)	22.31	24.19	22.45	24.95	22.25	24.96	22.70	25.34

Note. The same special ellipsoid slip surface (R_y=R_x, θ=0) used by Zhang is adopted in this paper.

Table 2: Comparisons of F and critical slip surface for Example 1 (Janbu's simplified method).

R_y (m)	24.4		48.8		73.2		97.6	
	Zhang	Current	Zhang	Current	Zhang	Current	Zhang	Current
F	2.068	2.066	1.971	1.961	1.951	1.938	1.944	1.929
X_c (m)	14.23	14.2	14.1	14.3	14.1	14.5	14.23	14.6
Z_c (m)	24.32	24.37	23.37	24.59	23.4	24.71	23.34	24.68
R_x (m)	21.34	21.67	20.97	22.48	21.03	22.87	20.91	22.78

Note. The same special ellipsoid slip surface (R_y=R_x, θ=0) used by Zhang is adopted in this paper.

Table 3: Comparisons of F and critical slip surface for Example 1 (Spencer's method).

R_y (m)	24.4		48.8		73.2		97.6	
	Zhang	Current	Zhang	Current	Zhang	Current	Zhang	Current
F	2.243	2.233	2.143	2.129	2.129	2.108	2.132	2.100
X_c (m)	13.5	13.9	13.6	14.0	13.1	14.01	13.36	13.9
Z_c (m)	26.99	25.62	28.05	25.71	28.4	24.11	28.44	26.99
R_x (m)	22.46	23.59	22.16	24.76	22.65	25.26	22.46	25.36

Note. The same special ellipsoid slip surface (R_y=R_x, θ=0) used by Zhang is adopted in this paper.

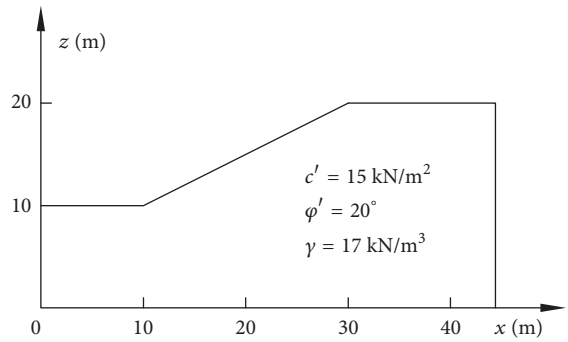

Figure 5: Geometry and properties of Example 2.

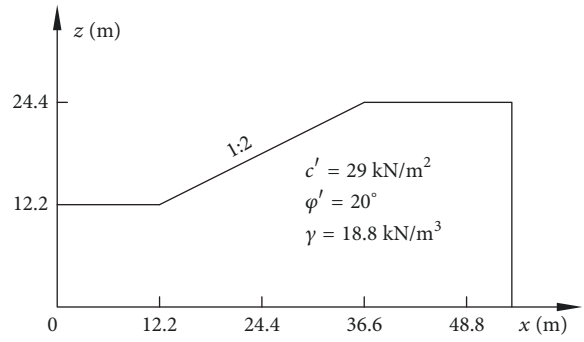

Figure 7: Geometry and properties of Example 3.

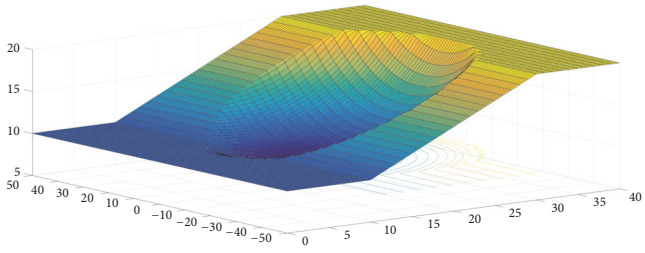

Figure 6: Critical slip surface for Example 2.

0.06%, respectively. The calculated unique DOS is equal to 0°, which is the same as Kalatehjari et al. [12].

Example 3. To further investigate the ability of the present method to determining the 3D shape and unique DOS of the critical slip surface, a hypothetical 3D slope problem is designed and analyzed. The geometry of Example 3 and its geomechanical properties are shown in Figure 7. This example involves four different 3D models, as shown in Figure 8. The unique DOS of the four cases can be predicted because the boundaries of slopes were constant and the face was rotated 10° clockwise in x-y plane in each step of the example. The minimum factors of safety should be equal to each other for all the models. Table 5 shows the minimum factors of safety and the unique DOS for all conditions. Figure 9 shows the critical slip surfaces for Example 3. The maximum difference between the unique DOS obtained by the present method and those logically estimated is less than 0.2°, which demonstrates the ability of the proposed method to determining the unique DOS of the critical slip surface. The minimum safety factors of the four models are not exactly equal to each other, but the maximum difference is less than 0.01%. This difference may be attributed to the discretization of the sliding mass and the different grid widths. This problem can be minimized by sufficiently small grid width. These results demonstrate the ability of the presented method to determining the 3D shape, minimum factor of safety, and unique DOS of the critical slip surface.

Example 4. Example 4 is selected to investigate the effects of the earthquake force and its direction on the minimum factor of safety and the unique DOS of the critical slip surface. The geometry of this example is symmetry about

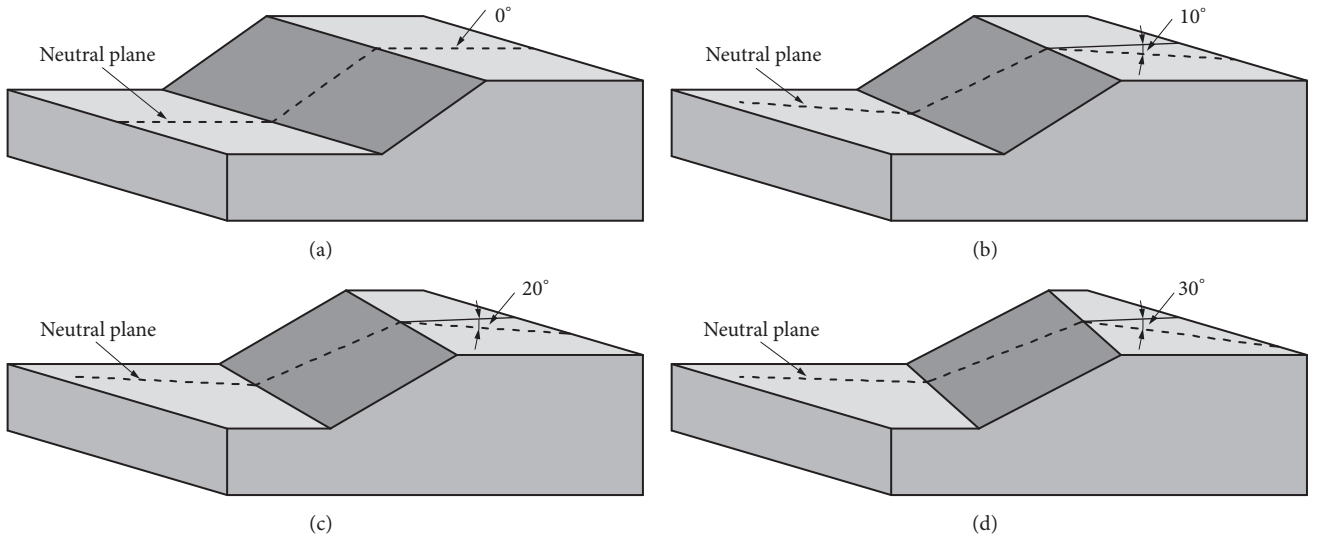

Figure 8: Three-dimensional model for Example 3.

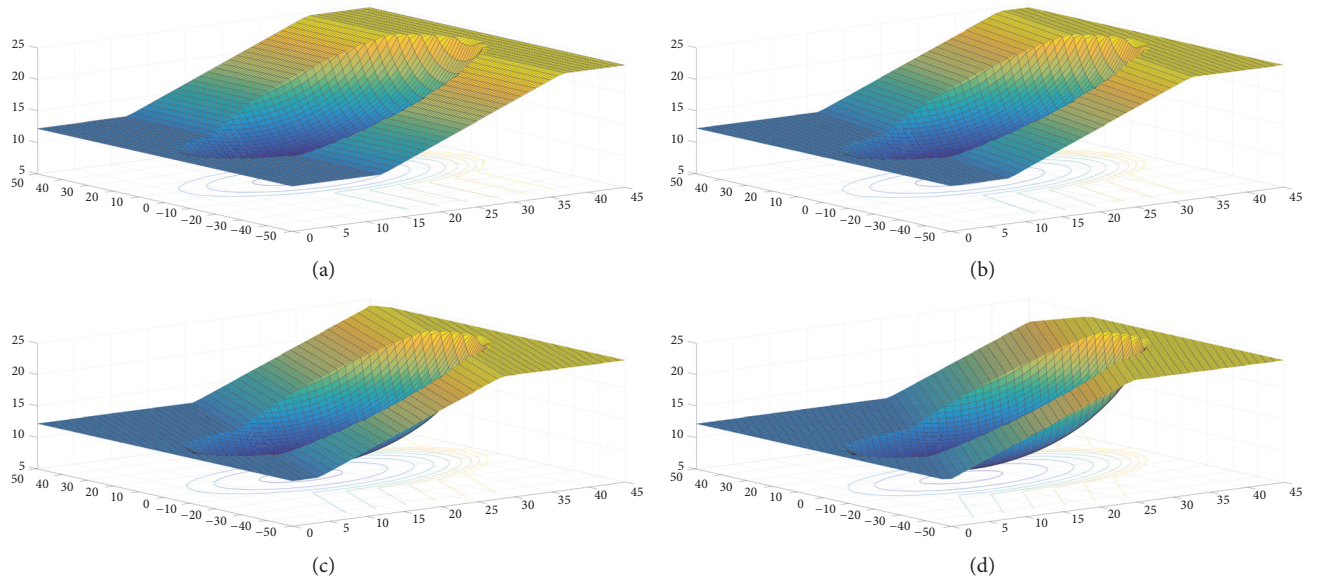

Figure 9: Critical slip surfaces for Example 3.

Table 4: Comparison of F for Example 2.

	F (2D)	F (3D)
Alkasawneh et al. [11]	1.70 (PLAXIS)	1.80 (PLAXIS)
Kalatehjari et al. [12]		1.77 (Bishop)
current(Ry=50)	1.697 (Spencer)	1.799 (Spencer)

Table 5: Comparison of F and DOS for Example 3.

model	Slope angle to x-axis(°)	F	Difference (%)	DOS	
				expected	obtained
1	0	2.1987	0.001	0.001	0.01
2	10	2.1989	0.009	10.00	9.80
3	20	2.1986	0.005	20.00	19.93
4	30	2.2000	0.056	30.00	29.94

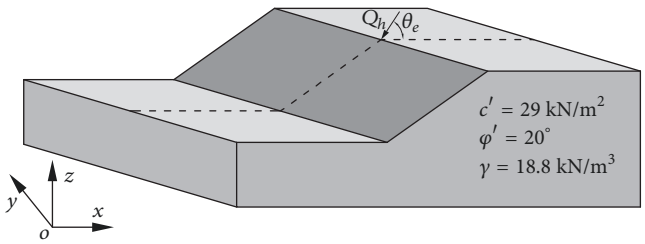

Figure 10: Three-dimensional model for Example 3.

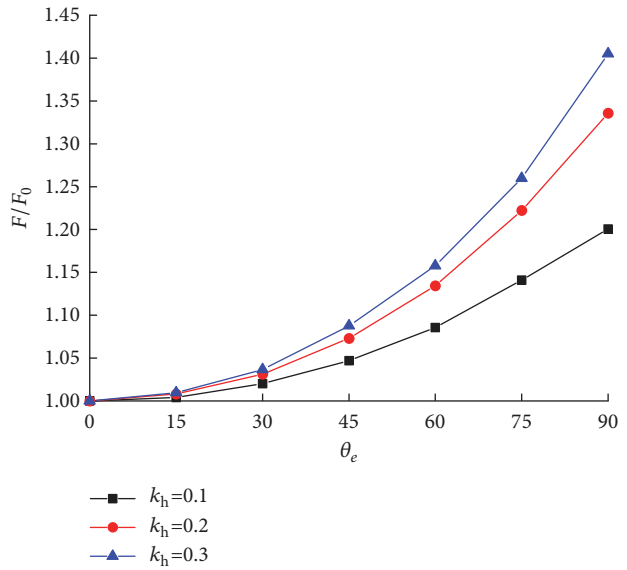

Figure 11: Difference of factor of safety with various θ_e.

the neutral plane, but the earthquake force acting on this slope is asymmetry as shown in Figure 10. The pseudo-static acceleration coefficient K_h is set equal to 0.1, 0.2, and 0.3, and the direction of the earthquake force θ_e ranges from 0° to 90°.

Figure 11 presents the difference in the factor of safety F/F_0 (where F is the factor of safety with variable θ_e, and F_0 is the factor of safety with θ_e =0) between considering and neglecting the direction of earthquake force. It can be seen from (5) that the components of seismic force in the direction of x-axis Q_{hxi} decrease the increase of θ_e. A smaller Q_{hxi} generates a failure surface with a larger factor of safety. Thus, the factor of safety increases with the increase of θ_e, as is shown in Figure 11. It can be seen that the difference in factor of safety (F/F_0) slightly increases as the direction of earthquake force increases when $\theta_e \leq 30^\circ$ and then tends to increase obviously. The direction of earthquake force (θ_e) has significant effects on the difference in factor of safety. Neglecting the effects of the direction of earthquake force on the factor of safety can lead to overestimation in 3D slope stability analysis. Typically, the difference can reach a maximum value of 40.5% when the direction of earthquake force θ_e=90° and the pseudo-static acceleration coefficient K_h=0.3.

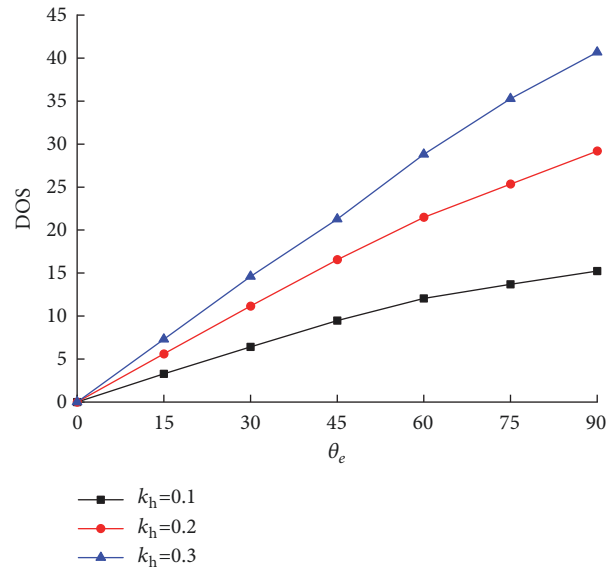

Figure 12: Results of DOS considering θ_e.

Figure 12 shows the effects of the direction of earthquake force (θ_e) on the unique DOS of the critical slip surface. It can be seen from (6) that the components of seismic force in the direction of y-axis Q_{hyi} increase with the increase of θ_e, which results in an increase of the DOS as is shown in Figure 12. When the earthquake force acts parallel to the x-axis (θ_e =0, Q_{hyi}=0), the DOS is equal to 0° which is the same as predicated. It can be seen that as θ_e and K_h increased, the value of the DOS increased linearly. Neglecting the effects of the direction of earthquake force (θ_e) can lead to miscalculation of the DOS of the critical slip surface. Typically, when θ_e=90° and K_h=0.3, the miscalculation of the DOS can be up to over 40°.

Figure 13 illustrates the difference in the unique DOS of critical slip surface between different geomechanical properties (c', φ'). The results of Figure 9 point toward the same trends that the unique DOS increases as the direction of earthquake force (θ_e) increases. It also found out that all the values DOS are consistent with each other, the maximum difference between which are less than 0.5°. It means that the geomechanical properties have little effects on the unique DOS of critical slip surface.

The calculated results indicated that the 3D analysis yields a conservative estimate for the factor of safety when the direction of the earthquake force is assumed to parallel to the x-axis. It is conservative because the effects of the direction of earthquake force are not included in the analysis. The 3D analysis neglecting the direction of earthquake force is appropriate for slope design because it yields a conservative estimate for the factor of safety. A 3D analysis considering the effects of direction of earthquake force is recommended for the backanalysis of 3D slope failures so that the back-calculated shear strength reflects the effects of direction of earthquake force. The backcalculated shear strength then can be used in remedial measures for failed slopes or slope design at sites with similar conditions.

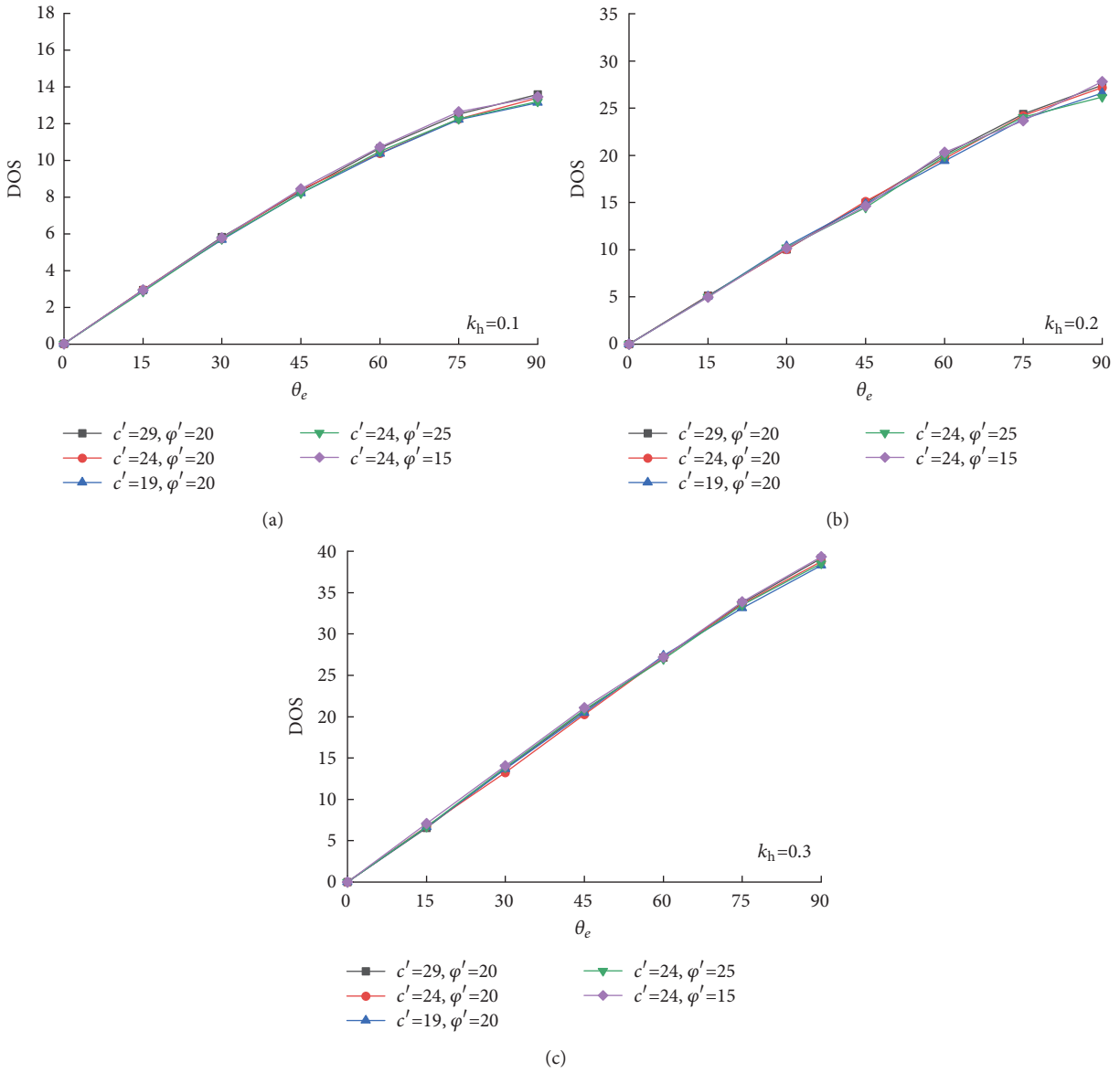

FIGURE 13: Effects of strength parameters (c', φ') on DOS: (a) $K_h = 0.1$, (b) $K_h = 0.2$, and (c) $K_h = 0.3$.

5. Conclusion

Simplified 3D Spencer's method with a random search technique was proposed to assess the stability of slopes under quasistatic load. A computer code was developed in Matlab to carry out the calculations. In addition, a meaningful comparison is made to investigate the effects of the direction of the earthquake force on the factor of safety and the DOS. Based on the results presented, the following conclusions can be made:

(1) The differences in factor of safety F/F_0 increase with an increase in the pseudostatic acceleration coefficient K_h and the direction of earthquake force θ_e values. Neglecting the effects of θ_e on the factor of safety can lead to overestimation in 3D slope stability analysis.

(2) The direction of earthquake force θ_e has obvious influence on the unique DOS of the critical slip surface. The DOS of the critical slip surface increases linearly with an increase in θ_e and K_h values.

(3) The effective cohesion c' and friction angle φ' of the soil have nearly no influence on the unique DOS of the critical surface.

Data Availability

The data used to support the findings of this study are available from the corresponding author upon request.

Conflicts of Interest

The authors declare that they have no conflicts of interest.

Acknowledgments

This study was financially supported by National Natural Science of Foundation of China (Grant nos. 41630638 and 51508160).

References

[1] A. W. Bishop, "The use of the slip circle in the stability analysis of slopes," *Géotechnique*, vol. 5, no. 1, pp. 7–17, 1955.

[2] N. Janbu, "Slope stability computations," *Embankment Dam Engineering-Casagrande Volume*, pp. 47–86, 1973.

[3] N. U. Morgenstern and V. E. Price, "The analysis of the stability of general slip surfaces," *Geotechnique*, vol. 15, no. 1, pp. 79–93, 1965.

[4] E. Spencer, "A method of analysis of the stability of embankments assuming parallel inter-slice forces," *Géotechnique*, vol. 17, no. 1, pp. 11–26, 1967.

[5] D. Leshchinsky and R. Baker, "Three-dimensional slope stability: end effects," *Soil & Foundations*, vol. 26, no. 4, pp. 98–110, 1986.

[6] O. Hungr, "An extension of Bishop's simplified method of slope stability analysis to three dimensions," *Géotechnique*, vol. 37, no. 1, pp. 113–117, 1987.

[7] O. Hungr, F. M. Salgado, and P. M. Byrne, "Evaluation of a three-dimensional method of slope stability analysis," *Canadian Geotechnical Journal*, vol. 26, no. 4, pp. 679–686, 1989.

[8] L. Lam and D. G. Fredlund, "A general limit equilibrium model for three-dimensional slope stability analysis," *Canadian Geotechnical Journal*, vol. 30, no. 6, pp. 905–919, 1993.

[9] C.-C. Huang and C.-C. Tsai, "New method for 3D and asymmetrical slope stability analysis," *Journal of Geotechnical and Geoenvironmental Engineering*, vol. 126, no. 10, pp. 917–927, 2000.

[10] Y. M. Cheng and C. J. Yip, "Three-Dimensional asymmetrical slope stability analysis extension of Bishop's, Janbu's, and Morgenstern–Price's techniques," *Journal of Geotechnical and Geoenvironmental Engineering*, vol. 133, no. 12, pp. 1544–1555, 2007.

[11] W. Alkasawneh, A. I. Husein Malkawi, J. H. Nusairat, and N. Albataineh, "A comparative study of various commercially available programs in slope stability analysis," *Computers & Geosciences*, vol. 35, no. 3, pp. 428–435, 2008.

[12] R. Kalatehjari, A. Arefnia, A. S. A. Rashid, N. Ali, and M. Hajihassani, "Determination of three-dimensional shape of failure in soil slopes," *Canadian Geotechnical Journal*, vol. 52, no. 9, pp. 1283–1301, 2015.

[13] C.-C. Huang, C.-C. Tsai, and Y.-H. Chen, "Generalized method for three-dimensional slope stability analysis," *Journal of Geotechnical and Geoenvironmental Engineering*, vol. 128, no. 10, pp. 836–848, 2002.

[14] R. Kalatehjari, A. S. A Rashid, M. Hajihassani, M. Kholghifard, and N. Ali, "Determining the unique direction of sliding in three-dimensional slope stability analysis," *Engineering Geology*, vol. 182, pp. 97–108, 2014.

[15] Y. Wan, Y. Gao, and F. Zhang, "A simplified approach to determine the unique direction of sliding in 3D slopes," *Engineering Geology*, vol. 211, pp. 179–183, 2016.

[16] C. L. Zhang, *Study on the three-dimensional limit equilibrium of slope stability. (PHD)*, Chang an University, 2008.

[17] H. B. Seed, "Considerations in the earthquake-resistant design of earth and rockfill dams," *Géotechnique*, vol. 29, no. 3, pp. 215–263, 1979.

[18] M. Garevski, Z. Zugic, and V. Sesov, "Advanced seismic slope stability analysis," *Landslides* , vol. 10, no. 6, pp. 729–736, 2013.

[19] A. Johari, S. Mousavi, and A. Hooshmand Nejad, "A seismic slope stability probabilistic model based on Bishop's method using analytical approach," *Scientia Iranica. Transaction A, Civil Engineering*, vol. 22, no. 3, pp. 728–741, 2015.

[20] R. Baker, R. Shukha, V. Operstein, and S. Frydman, "Stability charts for pseudo-static slope stability analysis," *Soil Dynamics and Earthquake Engineering*, vol. 26, no. 9, pp. 813–823, 2006.

[21] F. Zhang, Y. Gao, Y. Wu et al., "Effects of vertical seismic acceleration on 3D slope stability," *Earthquake Engineering and Engineering Vibration*, vol. 15, no. 3, pp. 487–494, 2016.

[22] Z. Y. Chen, "Random trials used in determining global minimum factors of safety of slopes," *Canadian Geotechnical Journal*, vol. 29, no. 2, pp. 225–233, 1992.

[23] Y. F. Gao, F. Zhang, G. H. Lei, and D. Y. Li, "An extended limit analysis of three-dimensional slope stability," *Géotechnique*, vol. 63, no. 6, pp. 518–524, 2013.